Effects of Active Site Inhibitors on APN-dependent Coronavirus Entry

A THESIS

SUBMITTED TO THE FACULTY OF

UNIVERSITY OF MINNESOTA

BY

Yijian Cai

IN PARTIAL FULFILLMENT OF THE REQUIREMENTS

FOR THE DEGREE OF

MASTER OF SCIENCE

Supervisor: Dr. Fang Li

June 2017

Acknowledgements

I would first like to express my sincere gratitude to my advisor Dr. Fang Li for the continuous support in my Master's study, for his encouragement and motivation during the difficult times in my research, and for his advice and help in my future career.

Besides my advisor, I would like to thank the rest of my thesis committee: Dr. Stanley A. Thayer from the Depart of Pharmacology, and Dr. Hinh Ly from the Department of Veterinary and Biomedical Sciences, for the time and effort reading and evaluating my work, and for their insightful comments and encouragement.

I thank my fellow labmates for their generous help with my work, for the sleepless night we were working together before deadlines.

Last but not least, I would like to thank my parents for their support of my livelihood and study in America.

Abstract

Aminopeptidase N(APN) has been shown as a receptor of several coronaviruses, such as HCoV-229E, TGEV, CCoV and FeCoV. Bestatin and Actinonin are inhibitors which can block APN enzymatic activity. These inhibitors bind to the catalytic site of APN, while viruses bind to the outer surface of APN. Here we investigate the mechanism of APN inhibition on protein-protein binding, receptor expression and coronavirus entry. We find that these chemical compounds can inhibit the protein-protein interaction between APN and Coronavirus spike; these inhibitors can also regulate APN RNA and protein expression; additionally, these compounds can inhibit the pseudovirus entry of HCoV-229E into human cells at a certain level. Additionally, coronavirus spike-treated human cells show a decrease in APN expression. This phenomenon may reveal an adaptation of cells to the different treatments and conditions. Our research may provide a new potential strategy for antiviral treatment.

Table of Contents

List of Tables

List of Figures

Introduction

Coronaviruses (CoV) are a group of enveloped, single-stranded, positive-sense RNA viruses which belong to *Coronavinae*, a subfamily of *Coronaviridae* in the order *Nidovirales*. They are the largest RNA viruses discovered to date, with genome sizes range approximately from 26 to 32 kilo-bases (kb).

Currently, coronaviruses are classified into four genera: Alpha (α), Beta (β), Gamma (γ) and Delta (δ) (1). Mammalian coronaviruses mainly belong to the genera of Alpha and Beta; avian coronaviruses all belong to the genera of Gamma and Delta. Several coronaviruses are pathogenic in humans and domestic animals, such as Human Coronavirus 229E (HCoV-229E) (2), Human Coronavirus NL63 (HCoV-NL63) (3, 4), Transmissible Gastroenteritis Virus (TGEV), Feline Coronavirus (FeCoV), Porcine Epidemic Diarrhea Virus (PEDV) and Canine Coronavirus (CCoV) in AlphaCoV; Coronavirus HKU1 (CoV-HKU1) (5), Human Coronavirus OC43 (HCoV-OC43) (6), Severe Acute Respiratory Syndrome coronavirus (SARS-CoV) (7, 8), Middle East Respiratory Syndrome Coronavirus (MERS-CoV) (9, 10), Mouse Hepatitis Virus (MHV) and Bovine Coronavirus (BCoV) in BetaCoV; Avian infectious bronchitis virus (IBV) in GammaCoV and porcine coronavirus HKU15 in DeltaCoV (11, 12). The coronavirus virion contains four major structural proteins: the spike (S), membrane (M), envelope (E) and nucleocapsid (N) protein. Trimer of S proteins forms the spike of CoV, which gives the virion the crown-like appearance under microscopy. The ectodomain of S protein consists of two subdomains, receptor binding S1 subunit and membrane-fusion S2 subunit (13). S1 is critical in receptor recognition and virus binding, providing receptor affinity, while S2 mediates the virus fusion and entry. Traditionally, two domains have been identified in S1: N-terminal domain (S1-NTD) and C-terminal domain (S1-CTD), distinguished by their location and functional differences. At least one of these two domains functions as the Receptor Binding Domain (RBD). S1-NTD usually recognizes

sugar receptor, and S1-CTD usually binds protein receptors (11, 14-16). Recent cyro-EM studies on S protein structure show that the S1 subunit contains 5 independent structural sub-domains, namely, "0", "A", "B","C", and "D". Although the absence of "0" domain is found in some CoVs, the "0" and "A" domain combined are thought to be associated with the sugar recognition. The domain "B" provides protein receptor affinity (17-21).

Coronaviruses recognize a variety of protein and sugar receptors. Most of the Alpha-CoVs utilize the APN as their receptor, especially feline APN (22). An exempt is HCoV-NL63, which utilizes the Angiotensin-converting enzyme 2 (ACE2), a protein receptor of SARS-CoV in BetaCoV. APN has been demonstrated to facilitate PEDV infection (16, 23-26), while there is still a debate whether APN functions as its receptor (27, 28). Other BetaCoVs, like MERS-CoV, which uses Dipeptidyl peptidase 4 (DPP4) as the receptor; MHV, recognizes CEACAM1. Sugar has been demonstrated to be the receptor of OC43, HCoV-HKU1, BCoV and IBV. Additionally, TGEV, PEDV and MHV also utilize sugar as co-receptor. Receptors of some coronaviruses are listed below (Table 1).

Table 1. Receptor recognition of some coronaviruses

Genera	CoV	Protein Receptor	Sugar Receptor/ Co-receptor
α	TGEV	APN(29)	Sialic acid (14, 15)
	PEDV	APN*	Sialic acid (16)
	FeCoV	APN(30)	/
	CCV	APN(30)	/
	HCoV-229E	APN(31)	/
	HCoV-NL63	ACE2(32)	/
β	SARS-CoV	ACE2(33)	DC-SIGN, DC-SIGNR(34)
	HCoV-OC43	/	Sialic acid (35)
	HCoV-HKU1	/	Sialic acid (36)
	MERS-CoV	DPP4(37)	/
	MHV	CEACAM1a(38, 39)	/
γ	IBV	/	Sialic acid (40)

*: There is still a debate whether APN is the receptor of PEDV.

/ : means unknown or unavailable.

TGEV is one of the most significant coronaviruses in swine. The virus, which can induce vomit and watery diarrhea among almost all classes of pigs, spreads rapidly and causes nearly 100% mortality in newborn piglets. TGEV mainly infects the small intestine of the host, which can lead to shortening of villi by reducing the number of absorptive cells. As a result, the infected pigs develop digestive disorder and finally die from dehydration. TGEV also provides the backbone of a novel Chimeric Swine Enteric Coronavirus (SeCoV) (41). In addition, porcine respiratory coronavirus (PRCV) (42) is known to be a mutant of TGEV.

229E is the first sequenced human CoV isolated in 1960s from patients with common cold (2). The virus infects a wide range of human regardless of gender, age or geographic areas. In most cases, HCoV-229E infection only raises mild cold-like

symptoms, such as nasal discharge, cough and headache (43). However, severe respiratory infections by HCoV-229E can also cause hospitalization in children, the elderly and immunocompromised patients (44). Titers of HCoV-229E antibodies usually decrease after one year infection, which indicates numerous infections of HCoV-229E during lifetime (45). Therefore, lacking treatment for HCoV-229E could induce substantial economic cost and decreased life quality.

Mammalian Aminopeptidase N (APN or CD13), a member of M1 family, is a zinc-dependent ectoenzyme, which is widely expressed on the surface of renal and intestinal epithelia cells, and in nervous system. APN modulates neutral peptides cleavage from N-terminus of various oligopeptides, also functions as the receptor of many coronaviruses and conducts cellular signaling (46). APN is a critical marker and target in cancer metastasis and angiogenesis (47, 48).

APN forms head-to-head homodimers, each monomer has four distinct domains. The N-terminus of the substrate binds to the zinc active site of APN (Figure 1A), the remaining residues of the substrate can be accommodated into APN’s spacious cavity, which is surrounded by the four domains of APN and can also be extended to accommodate peptides with more amino acids (49). As a member of M1-family, APN also has two conformations: the open catalytically inactive form and the closed catalytically active form. Coronaviruses bind to the region distant from the catalytic site. The "virus-binding motifs" (VBMs) on the surface of APN have been mapped (49) (Figure 1B): VBM1 (residues 283-292) for HCoV-229E, VBM2 (residues 728-744) for TGEV and VBM3 (residues 760-784) for FeCoV/CCoV (25, 49, 50).

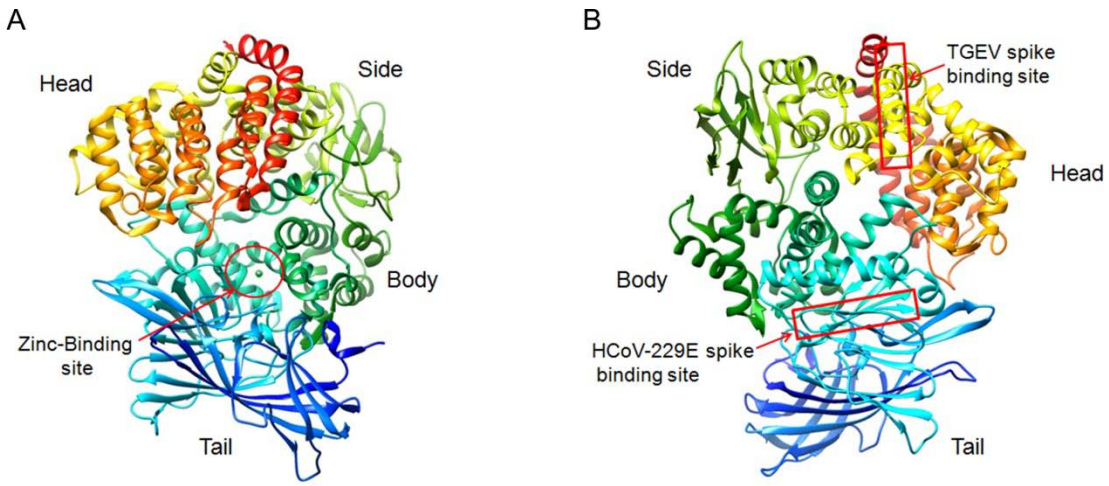

Figure 1. Structure of APN ectodomain and the binding sites (PDB ID: 4FKK) (49). (A) Four subdomains of APN ectromain are the head, side, body and tail domains. Substrates bind Zinc in the cavity surrounded by the four domains of APN. (B) Coronavirus-binding sites of HCoV-229E and TGEV.

Previously, it is commonly believed that coronavirus binding site is unrelated with the catalytic activity of APN, since APN mutants in active site or adding inhibitors (such as bestatin) do not interfere with coronavirus infection (26, 27, 51). However, a recent study shows that inhibitors anchoring active site will suppress virus binding by changing APN conformation (52).

Bestatin (Ubenimex), first isolated from the culture filtrate of *Streptomyces olivoreticuli* in 1976 (53), is the most widely used APN inhibitor. It is a competitive, reversible, slow-binding metalloprotease inhibitor which binds to catalytic site of APN. Actinonin, an antibacterial agent, was first isolated from a Malayan strain of *Actynomicetes*, and later also found to be an inhibitor of APN in 1985. In our research, we use TGEV and 229E spikes to investigate their relationship with APN in the presence or absence of active site inhibitors, and reversely, we also investigate the effect of these inhibitors on APN expression and virus entry.

Results and Discussion

Protein preparation

We aligned sequence of TGEV and HCoV-229E spikes with HCoV-NL63 (Genbank accession number YP_003767) (18) using Clustal Omega to identify the genes of interest (GOI) (Figure 2). GOI was amplified by overhang PCR using specific forward and reverse primers, in the PCR reaction, the restriction sites were added, and honeybee melittin signal peptide was fused to the N-terminus of GOI to increase the secretion efficiency. PFastBac 1 pre-inserted with IgG4 Fc sequence was used as the cloning vector (Figure 3). Briefly, both the template of interest and vector were digested by restriction enzymes and then ligated using DNA ligase. Recombinant plasmid was selected from ampicillin resistant colonies, and verified by diagnostic digestion and sequencing.

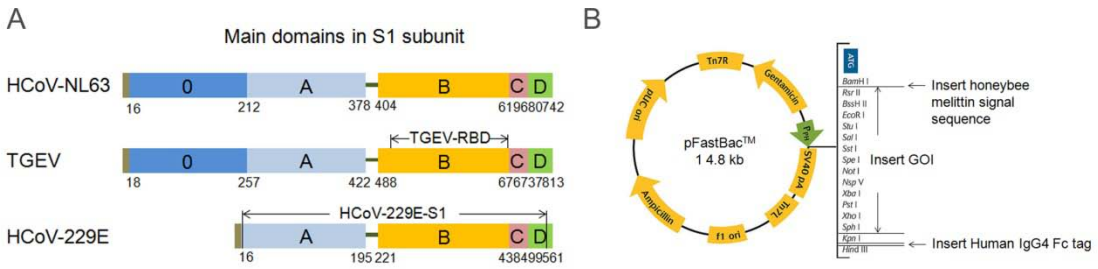

Figure 2. Recombinant plasmids preparation. A. Sequence alignment of TGEV and HCoV-229E with HCoV-NL63. We selected TGEV domain B and HCoV-229E S1 subunit as Genes of Interest (GOI); B. Map of recombinant plasmid. Honeybee melittin signal sequence was added to the N-terminus of the GOI by PCR, and Human IgG4 Fc sequence was inserted into the vector previously.

Proteins were expressed using Bac-to-Bac Baculovirus Expression Systems, and then purified using affinity column and gel filtration. The purified proteins were examined by SDS-PAGE, and the molecular weight of each protein was consistent with prediction (Figure 3).

To investigate whether inhibitors acting on APN catalytic site interfere with coronavirus binding, we purified truncated TGEV spike (residues 522-672) and 229E spike (residues 17-525) fused with Human IgG4 Fc tag, porcine APN (pAPN) ectodomain (residues 62-963) and human APN (hAPN) ectodomain (residues 33-967) fused with a C-terminal 6 Histidine sequence (His). We also used human ACE2 ectodomain (hACE2) (residues 19-615), human DPP4 (hDPP4) ectodomain (residues 39-766), SARS truncated spike (residues 306-527) and MERS truncated spike (residues 367-588) previously purified by lab colleagues (Figure 3).

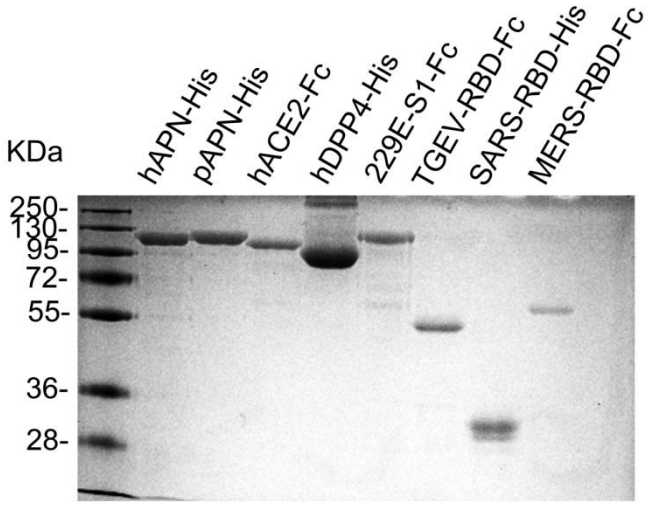

Figure 3. Proteins on SDS-PAGE. SDS-PAGE analysis of recombinant pAPN-His (Genbank accession number CAA82641.1), hAPN-His (Genbank accession number BC058928.1), hACE2-Fc (Genbank accession number AY623811), hDPP4-His (Genbank accession number NP_001926.2), 229E-S1-Fc (Genbank accession number NP_073551), TGEV-CTD-Fc (Genbank accession number CAA29175), SARS-RBD-His (Genbank accession number NC_004718) and MERS-RBD-Fc (Genbank accession number AFS88936.1).

Effects of catalytic inhibitors on binding interactions

To study the binding interaction between spike and APN, we used Dot blot Hybridization Assay (Table 2). Purified TGEV-RBD, HCoV-229E-S1, hAPN and pAPN ectodomain were used in all the binding affinity assays. The receptor of HCoV-229E is hAPN, while according to our experiment, HCoV-229E spike protein had higher affinity to pAPN than hAPN. Considering that pAPN and hAPN have 80% amino acid sequence identity, and pAPN matches well with hAPN in the ectodomain (Figure 4). We used pAPN instead of hAPN in HCoV-229E binding assays.

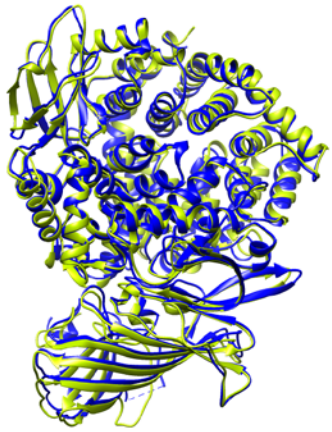

Figure 4. Match of pAPN and hAPN ectodomains. Match of pAPN ectodomain (in yellow) (PDB ID: 5LDS) with hAPN ectodomain (in blue) (PDB ID: 5LHD) by UCSF Chimera (52).

Table 2. Binding affinity of TGEV and HCoV-229E spike to APNs based on Dot Blot Hybridization Assay

Coronavirus spike	hAPN	pAPN
TGEV	-	++
HCoV-229E	+	++

- No binding affinity
+ Weak binding affinity
++ Strong binding affinity

Bestatin and actinonin are among the most widely used APN inhibitors, anchoring zinc-binding active site. Bestatin is a potent reversible inhibitor with IC50 of 16 μM (54-56). Actinonin is also a competitive inhibitor of APN with IC50 of 1.99 μM (57) . Same amount of TGEV or 229E proteins was added to the nitrocellulose membrane, and then incubated with pAPN with or without inhibitor (actinonin or bestatin) in working concentration (100 μM), respectively (Figure 5). We used MERS-CoV truncated spike as negative control (not shown). According to the results, in the presence of actinonin and bestatin, binding of both TGEV and HCoV-229E spike were attenuated. In addition, the bindings in actinonin treated proteins were weaker than bestatin treated ones, which was also corresponding to their affinity to APN.

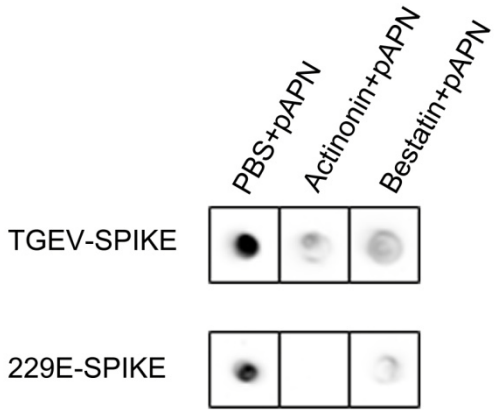

Figure 5. Dot Blot Hybridization Assay of TGEV and 229E spike with pAPN. pAPN was preincubated with PBS, actinonin or bestatin overnight. Bindings were detected using antibodies against C-terminal Fc tag;

We further used ELISA to study the binding interference of APN catalytic inhibitors (Figure 6). We saw that the inhibition of actinonin (Figure 6A) and bestatin (Figure 6B) was dose dependent. We also measured the binding affinity of SARS-CoV and MERS-CoV spike with hACE2 and hDPP4 in the presence of inhibitor, respectively. Sitagliptin is a catalytic inhibitor of DPP4. ELISA showed that sitagliptin did not decrease the binding of spike proteins to the receptor (Figure 6C), which was consistent with the previous reports showing that MERS-CoV entry could not be blocked by DPP4 inhibitors (58, 59). MLN-4760 is a potent ACE2 inhibitor anchoring the active site of ACE2 (60). In our result, SARS-CoV spike binding was unrelated with ACE2 inhibitor MLN-4760 (Figure 6D).

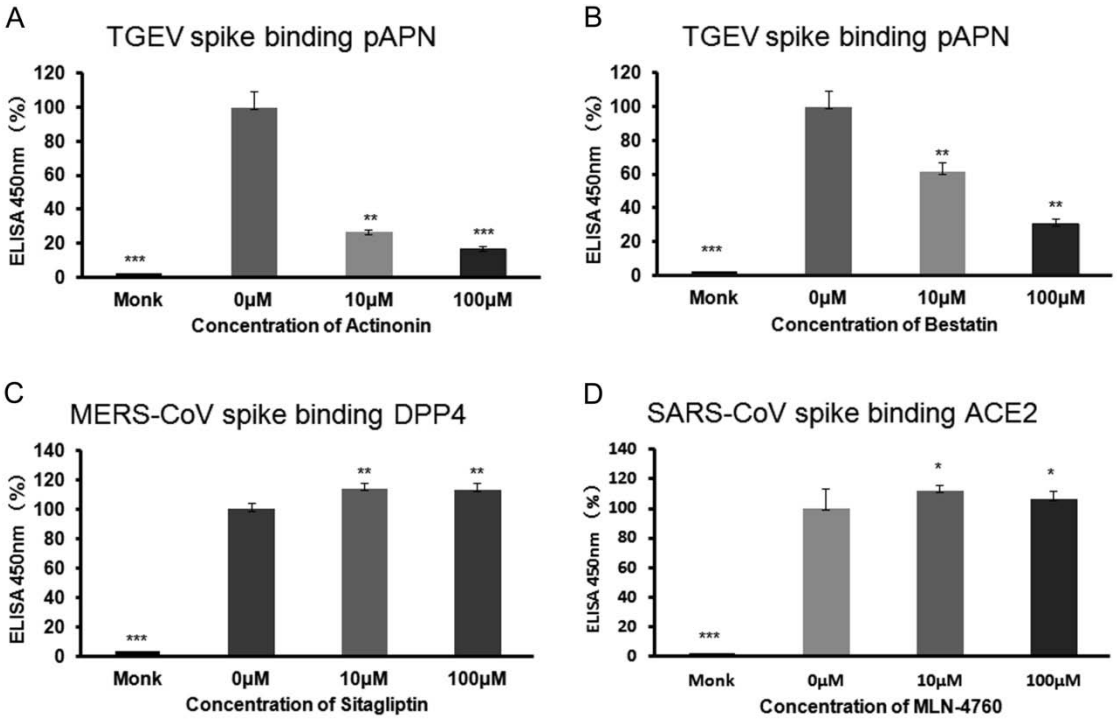

Figure 6. Interactions between spike and receptors in the presence of inhibitors. (A) (B) ELISA showing the binding interactions between TGEV spike and APN with or without inhibitors. The binding affinity of TGEV spike with pAPN in the absence of inhibitors was used as the standard and taken as 100%. Error bars indicate S.E. (compared with the standard two-tailed t test; *, $p<0.05$; **, $p<0.01$; ***, $p<0.001$, n=3). (C) (D) Binding of MERS-CoV spike with DPP4, and SARS-CoV spike with ACE2 in the presence or absence of inhibitors. The binding affinity of CoVs spike with receptors in the absence of inhibitors was used as the standard and taken as 100%. Error bars indicate S.E. (compared with the standard two-tailed t test; *, $p<0.05$; **, $p<0.01$; ***, $p<0.001$, n=6).

BLItz was used for the concurrent association of TGEV and 229E spike with APN. Affinity constants were shown in Table 3. Affinity constants of both TGEV and 229E spike remained unchanged regardless of the concentration of each protein. However, the association rate and maximum binding decreased with lower APN concentration when we fixed the concentration of spike (the spike was unsaturated) (Figure 7A). Then, we fixed both the concentration of spikes and APN. For both TGEV (Figure 7B) and HCoV-

229E (Figure 7C), the affinity constant (KD), association rate constant (ka) and dissociation rate constant (kd) were unchanged (Table 3), while the maximum association rate (V_{max}) and maximum binding decreased in the presence of bestatin. The decrease in binding rate reflected the decrease of free APN available for spike binding. In a word, bestatin could inhibit binding of spike and APN in a similar way as non-competitive inhibitors. For the association of MERS-CoV and hDPP4, bestatin did not change any affinity constants or binding rates (Figure 7D). In other words, bestatin did not have an effect on the binding between MERS-CoV spike and DPP4.

Table 3. Affinity constants for binding interactions

Coronaviruses spike	Receptors (μM)	Inhibitors (μM)	KD (M)	ka (1/Ms)	kd (1/s)	R^2
TGEV	0.0625 [a]	0	1.81e-8	3.00e5	5.44e-3	0.984
(50μg/ml)	0.25 [a]	0	1.90e-8	2.12e5	4.19e-3	0.988
	1 [a]	0	2.60e-8	1.21e5	3.16e-3	0.961
	0.25 [a]	25 [*]	5.34e-8	0.95e5	5.04e-3	0.993
	0.25 [a]	250 [*]	1.93e-8	1.53e5	2.96e-3	0.973
HCoV-229E	1 [a]	0	5.72e-8	6.26e4	3.58e-3	0.960
(50μg/ml)	1 [a]	25 [*]	7.98e-8	4.42e4	3.53e-3	0.966
	1 [a]	250 [*]	10.6e-8	5.64e4	9.16e-3	0.958
MERS-CoV	1 [b]	0	4.86e-7	3.00e5	5.44e-3	0.998
(50μg/ml)	1 [b]	250 [*]	8.34e-7	6.27e3	5.23e-3	0.995
	1 [b]	250 [#]	8.80e-7	2.12e5	4.19e-3	0.999

a: pAPN;

b: hDPP4;

*: Bestatin;

#: Sitagliptin

K_D (M) - Measured affinity of interaction; affinity constant in Molar;

ka (1/Ms) - Association rate constant;

kd (1/s) - Dissociation rate constant;

R2 value reports goodness of fit.

Likewise, we measured the affinity constants of MERS-CoV spike with hDPP4 using BLItz (Figure 7E). In the presence of sitagliptin, the affinity constants, as well as V_{max} and maximum binding did not change (Table 3). The active site inhibitor sitagliptin did not inhibit spike-receptor binding.

A

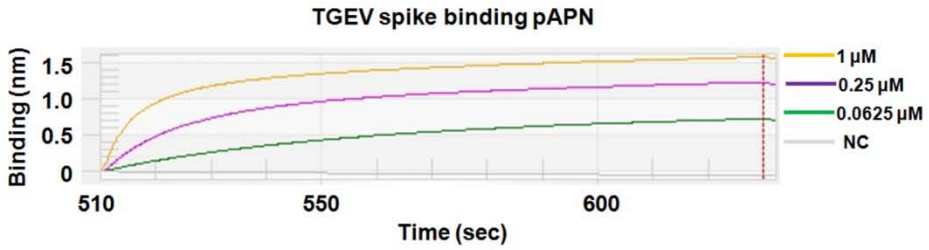
TGEV spike binding pAPN
Binding (nm)
1.5
1.0
0.5
0
510
550
600
Time (sec)
1 μM
0.25 μM
0.0625 μM
NC

B

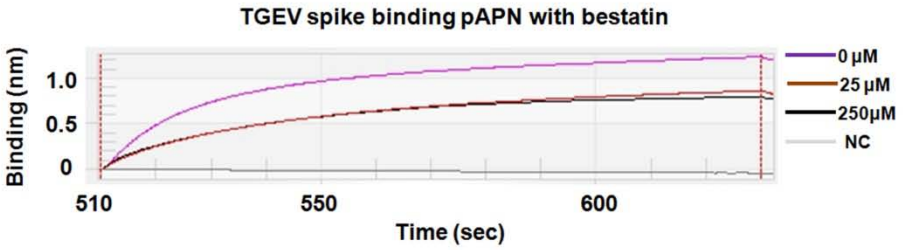
TGEV spike binding pAPN with bestatin
Binding (nm)
1.0
0.5
0
510
550
600
Time (sec)
0 μM
25 μM
250μM
NC

C

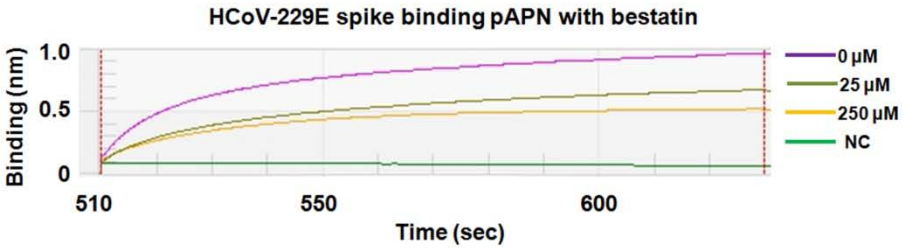
HCoV-229E spike binding pAPN with bestatin
Binding (nm)
1.0
0.5
0
510
550
600
Time (sec)
0 μM
25 μM
250 μM
NC

D

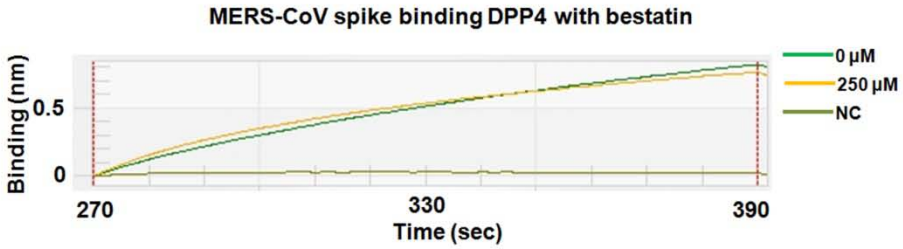
MERS-CoV spike binding DPP4 with bestatin
Binding (nm)
0.5
0
270
330
390
Time (sec)
0 μM
250 μM
NC

E


MERS-CoV spike binding DPP4 with sitagliptin
Binding (nm)
0.5
0
270
330
390
Time (sec)
0 μM
250 μM
NC

Figure 7. Concurrent binding between CoV spikes and receptors by BLItz. Sensors loaded with coronavirus spike. The data were shown using global curve fitting automatically by the system from the start of association. (A) Binding of TGEV spike with pAPN. The concentrations of TGEV were 50 μg/ml, pAPN were 1 μM, 0.25 μM and 0.0625 μM. (B)(C) Binding of TGEV spike or HCoV-229E spike with pAPN in the presence of Bestatin. The concentrations of bestatin were 0μM, 25μM and 250 μM. The concentrations of TGEV and HCoV-229E spike were 50 μg/ml. (D) Binding of MERS-CoV spike with DPP4 in the presence of Bestatin. The concentration of MERS-CoV spike was 50 μg/ml. The concentrations of bestatin were 0 μM and 250 μM. 250 μM of Bestatin in PBS was used as a negative control. (E) Binding of MERS-CoV spike with DPP4 in the presence of sitagliptin. The concentrations of sitagliptin were 0 μM and 250 μM. 250 μM of sitagliptin in PBS was used as a negative control.

Effects of APN inhibitors and spikes on APN expression

Apart from spike binding, the density of APN in cells may also contribute to viral entry. To investigate whether APN inhibitor have an effect on APN expression in cells, we treated human cells with bestatin and checked APN expression by Western blot and quantitative polymerase chain reaction (qPCR). First, we treated Huh 7 cells with bestatin at different concentrations (Figure 8A). At the concentration of 100 μM, a significant decrease of APN expression level was shown. We then chose 100 μM as the working concentration in the following experiments.

To study the effect of inhibitors on APN expression with time, we treated Huh 7 cells with bestatin (100 μM) in 10% FBS supplemented DMEM, and analyzed APN expression from 0 to 24 hours after treatment. For the first 2 hours post-treatment, a slight increase of APN expression was found after bestatin or actinonin treatment, followed by a decrease overtime (Figure 8B). Similarly, qPCR (Figure 8D) showed an increase in RNA 2 hours after treatment. The RNA rising in the early stages of inhibitors treatment was consistent with the increase of APN. Later, APN expression dropped. The fluctuation in RNA transcription may not be the dominant factor of the decreased APN in protein level. Other factors may play a role in the APN reduction.

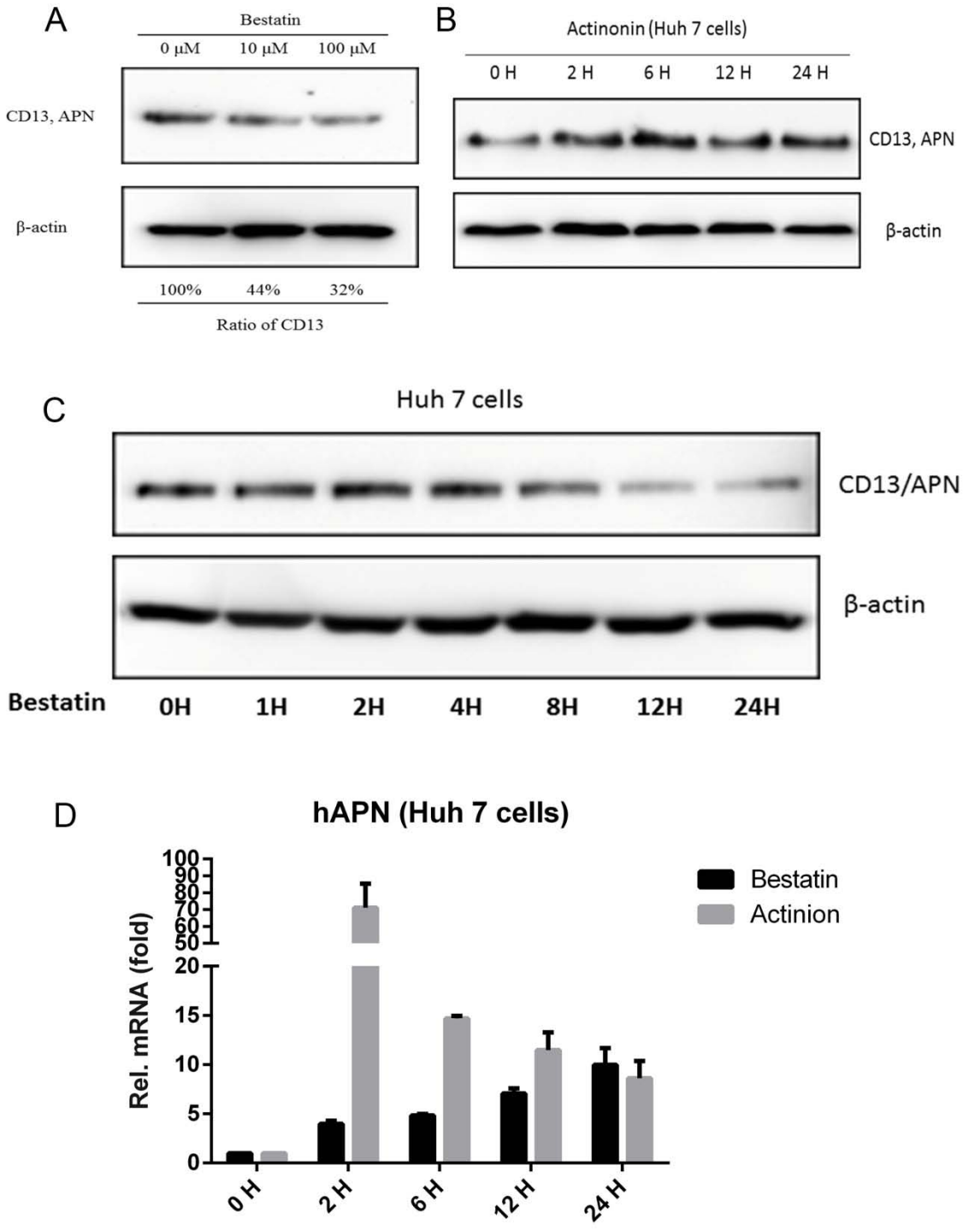

Figure 8. Effects of bestatin and Actinonin on APN expression in Huh7 cells. (A) Western blot showing the effects of bestatin on APN expression at different concentrations. Huh7 cells were treated with bestatin for 24 hours. APN was detected in cell lysates. (B) Western blot

showing the effects of actinonin on APN expression at (100 μM) at different time points post-treatment. APN was detected in cell lysates. APN was detected in cell lysates. (C) Western blot showing APN expression in Huh7 cells after bestatin treatment(100 μM) at different time points. APN was detected in cell lysates. β actin was used as the internal reference. (D) Effect of actinonin and bestatin on APN transcription levels by qRT-PCR. GAPDH was used as the internal reference.

It has been reported that SARS-CoV is related with ACE2 downregulation upon infection on lung cell surface (61). To investigate whether HCoV-229E or TGEV spike has a similar effect on APN, we treated cells with spikes (Figure 9), and detected the change of APN expression levels at different time points. Huh7 cells was treated with HCoV-229E spike, and HEK 293T-pAPN cells treated with TGEV spike. Under the treatment of spikes, APN expression decreased over time.

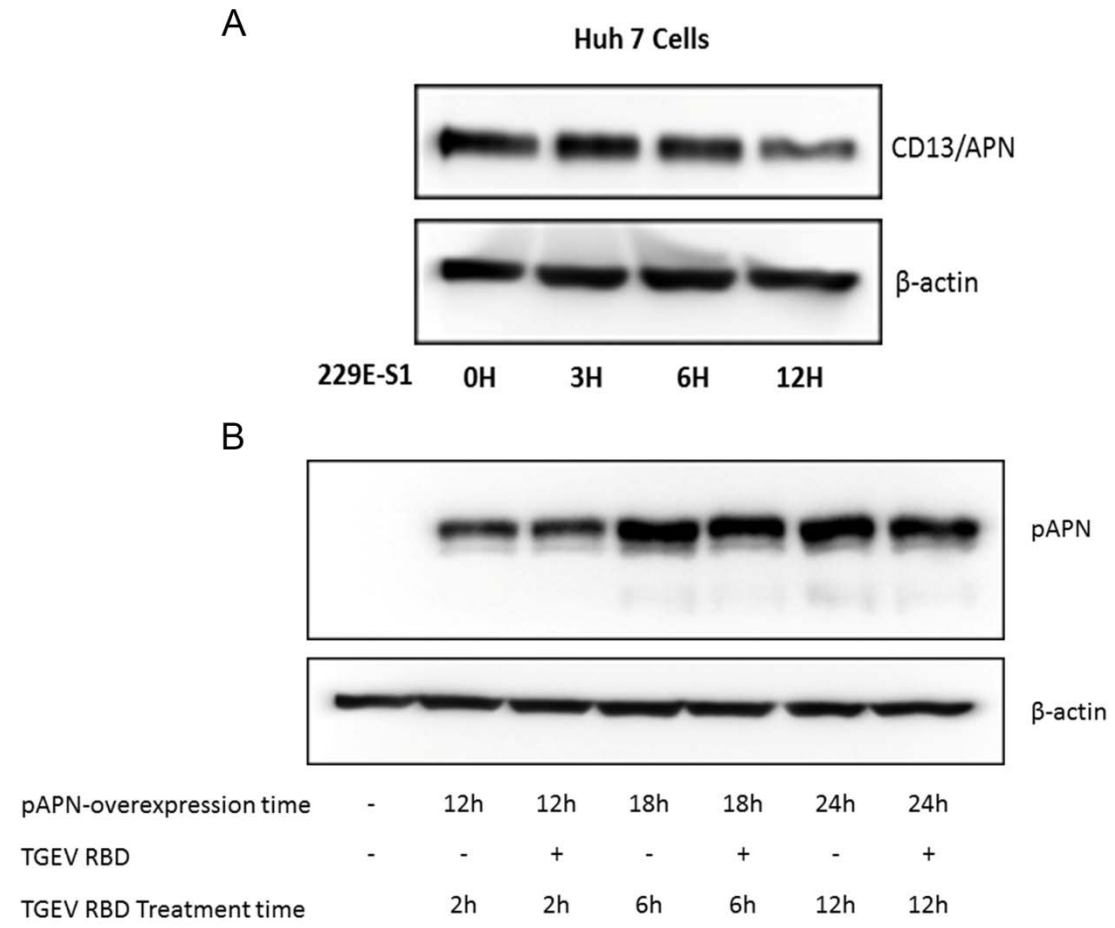

Figure 9. Effects of HCoV-229E and TGEV spike on APN in cells. (A) Effects of HCoV-229E spike (20 μg/ml) on APN in Huh7 cells at different time points. (B) Effects of TGEV spike (20 μg/ml) on APN in 293T/ pAPN cells at different time points. APN was detected in cell lysates by western blot. β-actin was used as the internal reference.

Effects of APN inhibitors on pseudovirus entry

To further confirm the influence of bestatin on viral entry, we did pseudotype assay of HCoV-229E. HEK 293T cells expressing human, porcine, feline and bat APN were used to confirm the receptor of HCoV-229E. According to the results, HCoV-229E pseudovirus could infect 293T cells with hAPN, pAPN and fAPN (Figure 10A). Huh7 cells were used for pseudovirus entry of HCoV-229E. After bestatin treatment for 24 hours, nearly 30% of the infection was prohibited (Figure 10B).

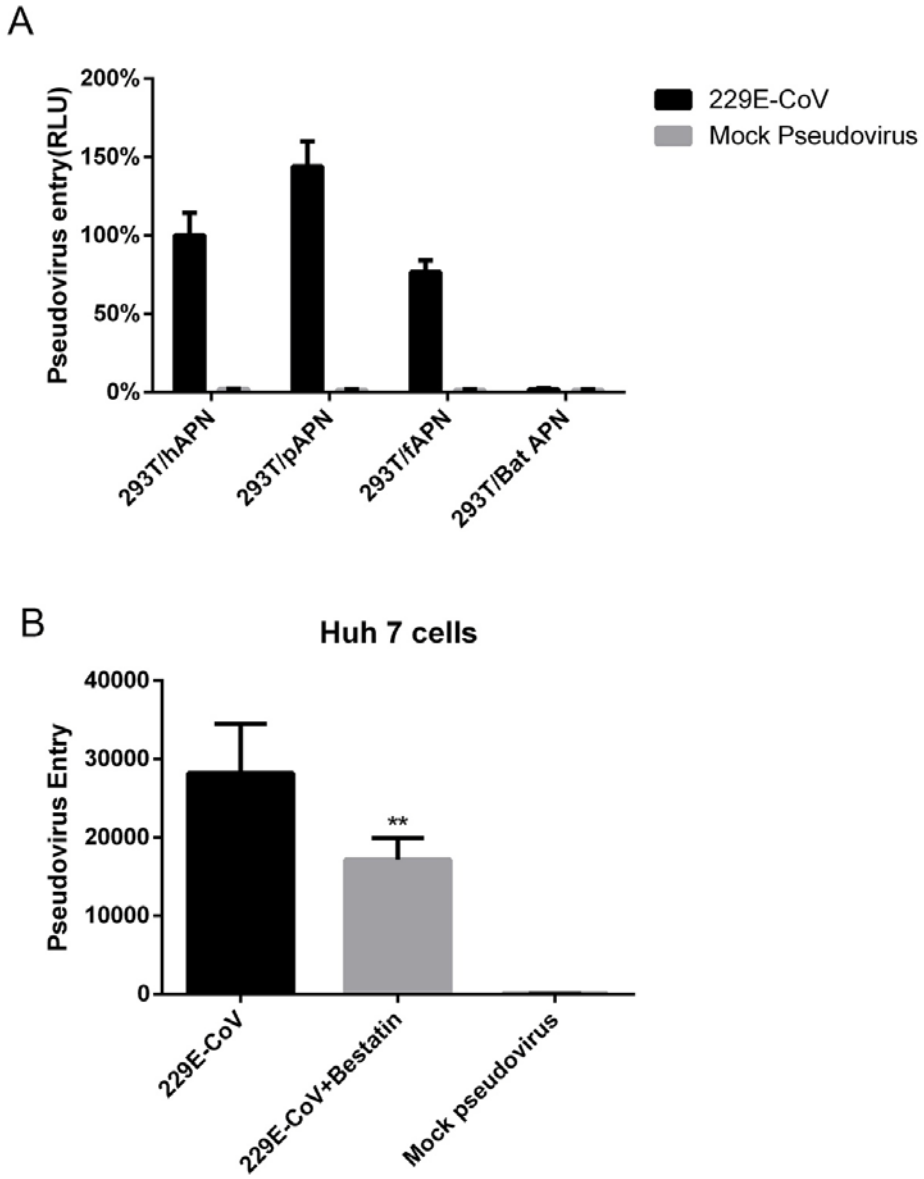

Figure 10. Effect of bestatin on HCoV-229E pseudovirus entry. (A) Pseudotyped HCoV-229E entry into cells expressing different receptors. The pseudovirus entry of HCoV-229E to 293T/hAPN was used as the standard and taken as 100%. (B) Effect of bestatin on HCoV-229E pseudovirus entry into Huh7 cells. Error bars indicate S.E. (compared with the standard two-tailed t test; *, $p<0.05$; **, $p<0.001$; n=4).

Discussion

Receptor binding is the first and most significant step in coronavirus infection. Structure studies during the last decade had revealed some interactions between coronavirus spikes and receptors (49, 50, 62). It is commonly believed that catalytic activity of APN is not associated with coronavirus binding (51), therefore, catalytic inhibitors of APN would not interfere with coronavirus entry. However, recent studies have indicated that these inhibitors may have some impact on the interaction between APN and coronavirus spike, such as TGEV and pAPN (52). However, limitted researches have ever been conducted using APN and coronavirus spike proteins. Our research has determined the binding affinity of 229E or TGEV spike with pAPN, and further elucidated the inhibition effect of catalytic inhibitors of APN like bestatin or actinonin on spike-receptor binding. According to some literature, the binding sites of coronavirus spike and APN catalytic inhibitors are different. However, our studies indicate that these inhibitors may play a role in the interaction between APN and coronavirus spike, the inhibitors might interfere with the coronavirus binding sites of APN. Our results are consistent with a previously report that these inhibitors probably hinder APN transition to the virus-specific open form (52), and consequently, the APN is no longer available to bind coronavirus spike. In addition, overdosed inhibitors could not completely block the spike binding, which might account for the reversibility of the inhibitors. APN binds Bestatin in a rapidly reversible process (63). As a result, free APN for spike binding is always available. A competition between spike and inhibitor in APN binding may also exist.

ACE2 and DPP4 are also metalloenzymes and receptors for coronavirus (64, 65), while according to our results, inhibitors binding to the active sites of these proteins do not block the binding of coronavirus.

The effect of APN catalytic inhibitors might be affected by many factors, such as binding affinity and receptor density. It is unknown which one is the determinant factor for the effect of the inhibition of pseudovirus entry. As mentioned above, APN active site inhibitors also function as reversible inhibitors of spike binding to APN. Moreover, APN inhibitors also have some effect on the expression of APN. The early-stage RNA rising

may be responsible for the increase of APN protein under the treatment of inhibitors. It is unknown the detailed mechanism of the enhancement of gene expression in the early time when treated with these inhibitors. In the late stage of bestatin or actinonin treatment, the APN protein decreased, however, the transcription of APN did not. Therefore, other factors might account for the reduction of APN in the late stages of the treatment of these inhibitors. More studies should be done to reveal the underlying mechanism of the APN reduction in the treatment of its inhibitors. Considering the function of APN, the reduction of APN might account for the endocytosis, phagocytosis or degradation (46).

Similar to SARS-CoV, the spike of HCoV-229E and TGEV could also reduce APN expression in cells (61). The cells might utilize the strategy to decrease their receptor density to protect them from virus infection. The cell surface expression of the chemokine receptors is regulated through their interaction with membrane trafficking pathways in their role as virus receptors. Similarly, spike protein may induce APN internalization and down modulation through unknown ways, which needs further studies (66). The cells may have evolved these mechanisms as an adaptation to the different conditions.

In conclusion, our study demonstrates the effect of APN enzymatic inhibitors on spike-receptor binding, APN expression and pseudovirus entry. These findings will provide a new potential strategy towards antiviral therapy.

Materials and Methods

PBS:	NaCl 8.00 g, KCl 0.20 g, Na_2HPO_4 1.44 g, KH_2PO_4 0.24 g, pH 7.4 (1000 mL).
PBST:	PBS+0.05% Tween-20
NaN3 Stock:	20% NaN_3 (1000 mL).
Buffer A1:	NaCl 29.22 g, KCl 0.20 g, Na_2HPO_4 1.44 g, KH_2PO_4 0.24 g, Imidazole 0.34 g, NaN_3 Stock 1 mL, pH 7.4 (1000 mL).
Buffer B1:	NaCl 29.22 g, KCl 0.20 g, Na_2HPO_4 1.44 g, KH_2PO_4 0.24 g, Imidazole 34.0 g, NaN_3 Stock 1 mL, pH 7.4 (1000 mL).
Buffer A2:	Tris-base 2.42 g, NaCl 29.22 g, NaN_3 Stock 1 mL, pH 7.4 (1000 mL).
Transfer buffer:	Tris-base 3.02 g, Glycine 14.26 g, 20% Methanol (V:V)
Running buffer:	Tris-base 3.02 g, Glycine 18.80 g, SDS 10.00 g (1000 mL).
Distaining buffer:	Distilled water 450 mL, Methanol 450 L, Acetic acid 100 mL.
Coating buffer:	Na_2CO_3 1.59 g; $NaHCO_3$ 2.94 g, pH 9.6. (1000 ml);
Blocking buffer:	PBS+5% Milk;
Diluted buffer:	PBST+1% Milk;
Stopping solution:	2M H_2SO_4;
Cell lysis buffer:	NaCl 11.68 g, Triton X-100 1.0% (V:V), Tris Base 6.05 g, pH 8.0.

Protein Preparation

Polymerase Chain Reaction(PCR): Genes of interest (GOI) were amplified by overhang PCR using specific forward and reverse primers (listed in Table below). Honeybee melittin signal peptide was fused to the N-terminus of GOI to increase the secretion efficiency. The primers were designed adding restriction site, and tagged with 6 Histidines (only receptors) in the C-terminus of GOI. Overhang PCR was operated on Eppendorf® Mastercycler. The PCR conditions were initial denaturation 5minutes at 95°C, cycle denaturation for 30 seconds at 95°C, and annealing for 30 seconds (between 48-72°C), extension for 5 minutes at 72°C, and final extension was at 72°C for 10min (30 cycles). DNA fragments with GOI were separated by agarose gel electrophoresis (140V for 20 minutes) and extracted by QIAquick Gel Extraction Kit (QIAGEN, Hilden, Germany).

Table 4. Reaction mixture of PCR

Component	Volume
10×pfu buffer	10 µl
Pfu^{TM} ultra II fusion HS DNA Polymerase (2.5 U/µl)	2 µl
Template DNA (100 ng/µl)	2 µl
Forward primer (10 ng/µl)	10 µl
Reverse primer (10 ng/µl)	10 µl
dNTP mix (2.5 mM each NTP)	8 µl
H_2O	58 µl
Total reaction volume	100 µl

Table 5. Primers for TGEV and HCoV-229E spike

GOI	Forward Primer	Reverse Primer
TGEV spike	ATAGGATCCATGAAATTCTT AGTCAACGTTGCCCTTGTTT TTATGGTCGTGTACATTTCTT ACATCTATGCTTCATTTTACA CTCATACAATCGTGA	ATAGGTACCTCCACT TCCACCATTGTCAGA GGGCACGC
HCoV-229E spike	ATAGGATCCATGAAATTCTT AGTCAACGTTGCCCTTGTT TTTATGGTCGTGTACATTTC TTACATCTATGCTCAGACCA CCAACGGCCTGAA	ATAGGTACCGGAGAA GCCGTAGGAGGTGA

Recombination DNA plasmid of porcine Aminopeptidase N ectodomain (pAPN), human Aminopetidase N ectodomain (hAPN), human Angiotensin-Converting Enzyme 2 ectodomain (hACE2), human Dipeptidyl peptidase-4 ectodomain (hDPP4), MERS-CoV spike (MERS spike), and SARS-CoV spike (SARS spike) were constructed previously.

Table 6. Sequence information of purified proteins

Protein	Genbank accession number	Residues	Tag
TGEV spike	CAA29175	522-672	Human IgG4 Fc
HCoV-229E spike	NP_073551	17-525	Human IgG4 Fc
SARS-CoV spike	NC_004718	306-527	His_6
MERS-CoV spike	AFS88936.1	367-588	Human IgG4 Fc
pAPN	CAA82641.1	62-963	His_6
hAPN	BC058928.1	33-967	His_6
hACE2	AY623811	19-615	Human IgG4 Fc
hDPP4	NP_001926.2	39-766	His_6

Digestion and Ligation: Both PCR products and vectors were digested by High Fidelity (HF ™) Restriction enzymes in CutSmart TM Buffer (New England Biolabs (NEB), Ipswich, MA) at 37°C for 1 hour, separated by gel electrophoresis and extracted by QIAquick Gel Extraction Kit. Digested GOI was inserted into the vector by T4 DNA ligase (NEB), incubated at 16°C overnight. After chilled on ice for 10 minutes, the mixture was added to 50μl of competent cells (NEB DH5αTM Competent E.coli), gently flicked and placed on ice for 30 minutes. After heat shock in a 42°C water bath for 30 s, the cells were placed on ice for another 5 minutes. 900 μl of SOC was added and then incubated in a incubator shaker at 250 rpm, at 37°C for 1 hour. Subsequently, the cells were centrifuged, resuspended in 100 μl of SOC buffer, and then spread on LB agar plates containing Ampicillin (50 μg/ml). After incubated at 37°C overnight, individual bacterial colonies was picked and amplified in 4ml of LB broth containing ampicillin (50 μg/ml). Plasmid was extracted from the overnight bacterial culture by QIAprep® Spin Miniprep Kit. Correct recombinant plasmids were determined by diagnostic restriction digestion and sequencing.

Transposition: The recombinant plasmid was added to 100 μl competent cells (NEB DH10BacTM Competent cells). The mixture was gently flicked and placed on ice for 30

minutes. After heat shock in a 42°C water bath for 45s, the mixture was place on ice for another 5 minutes, added 900 μl of SOC and incubated in a incubator shaker at 225 rpm, at 37°C for 5 hours. The cells were then spread on LB agar plates containing kanamycin (50 μg/ml), gentamicin (7 μg/ml), tetracycline (10 μg/ml), Bluo-gal (100 μg/ml), and IPTG (40 μg/ml). After incubated at 37°C for 48 hours, single white colonies were picked and streaked on fresh LB agar plates as above, and incubated at 37°C overnight. The confirmed single colony was inoculated into 5ml of LB broth containing kanamycin (50 μg/ml), gentamicin (7 μg/ml), and tetracycline (10 μg/ml). Recombinant bacmid DNA was subsequently extracted from the 24-hour liquid culture by Miniprep Kit.

Transfection： Sf9 insect cells in log phase (1.5-2.5 × 10^6 cells/ml) were diluted to 8 × 10^6 cells/ml in SF-900TMIII insect culture medium and plated 2ml (1.6× 10^6 cells) into each well of a 6-well plate. The cells were allowed to attach for 15 minutes at room temperature in the hood. For each bacmid to be transfected, 6 μl of Cellfectin® II Reagent (Invitrogen, Carlsbad, CA) and 6μl of bacmid were separately diluted in 100 μl medium and then mixed by inverting the tubes 3 times. The medium in the 6-well plate was removed and replaced with the DNA-Lipid mixture. After incubated at 27°C for 5 hours, the mixture was removed and replaced with 2 ml of SF-900TMIII insect culture medium containing 100 units/ml penicillin, and 100 μg/ml streptomycin. After incubated at 27°C for 72 hours, baculovirus-containing supernatant in passage 1 (P1) was transferred to sterile tubes, aliquoted and stored at -80°C. Baculovrius was gradually amplified by Passage 2 (P2), Passage 3 (P3) and Passage 4 (P4). P2 was directly made by adding 500 μl of P1 stock to 30 ml of SF9 cells in log phase growing in a 50 ml shake flask. Expression of the protein was detected by Western blot. After 7 days, the cell culture was transferred to 50 ml centrifuge tubes, spun at 6000 g for 20 minutes at 4°C in the swinging bucket rotor. Aliquots of the supernatant were frozen at -80°C. To make P3, 5 ml of P2 supernatant was transferred to 300 ml of SF9 cells in log phase growing in a 500 ml shake flask. Supernatant was collected by centrifuge after 7 days. Then, 150 ml of P3 supernatant was transferred to 1800 ml of sf9 cells in two 2 L shake flasks to make P4. Cell culture was collected once reaching a 40%-50% mortality rate (usually after 3 days).

Western blot: Protein expression was detected in P1 and P2 supernatant in day 3. Briefly, 30 μl of the cell culture was transferred to 1.5 ml tubes. Cells were harvested by spinning at 3,000 rpm for 5 minutes using the microfuge. The supernatant was transferred to another tube for further analysis. Proteins in each sample were separated by SDS-PAGE and transferred onto a PVDF membrane (Bio-Rad Laboratories, Hercules, CA). Membranes were blocked in PBST containing 5% non-fat milk for 1 hour at room temperature, and incubated with appropriate primary antibodies in PBST+2% non-fat milk for 3 hours at room temperature. The blots were washed three times for 10 minutes each with PBST and then incubated for 1 hour in room temperature with secondary antibodies in PBST+2% non-fat milk. After washed sufficiently, Amersham™ ECL™ Prime Western Blotting Detection Reagent (GE Healthcare, Boston, MA) was applied on the blot. The signal was detected using myECL™ Imager (ThermoFisher, Waltham, MA).

Samples preparation: P4 supernatant in day 3 was collected by spinning at 6000 g for 20 minutes in two 1L centrifuge bottles, and condensed in a concentrator to about 50-100 ml at 4°C. The condensed supernatant was filtered by 0.2 μm bottletop filter. Proteins were purified by affinity column, followed by gel filtration.

Affinity chromatography: 5 ml HiTrap™ nickel-chelating HP column (GE Healthcare) was used for protein with His_6 tag. The column was washed with 60 ml of distilled water, followed by 40 ml of 0.05 M EDTA, 20 ml of 0.1 M NiCl2, 60 ml of distilled water and 100 ml of PBS. The prepared protein-containing samples was pumped onto the column at 5 ml/min, and washed with 50 ml of PBS buffer. Proteins was eluted by elution buffer (buffer A1 and buffer B) containing gradient imidazole using AKTA. Fractions was detected by coomassie blue staining method. 5 ml HiTrap™ Protein A HP column (GE Healthcare) was used for protein with Fc tag. The column was washed with distilled water, followed by 20 ml of PB buffer. The prepared protein-containing samples was pumped onto the column at 5 ml/min, and washed with 50 ml of PB buffer. Proteins was eluted by 1M citric acid (pH=3.5) and immediately neutralized by 1 M Tris-Base (pH=9). The purified fractions was detected by coomassie blue staining method.

Gel filtration: About 0.5 ml of condensed protein samples was loaded to HiLoad Superdex 200 PG column (GE Healthcare) by syringe. Fractions were detected by coomassie blue staining method. Fractions containing target protein were collected and condensed using Amicon® Ultra centrifugal filters (Merk Millipore, Billerica, MA). The concentration of purified protein was measured using NanoDrop. The protein was aliquoted and frozen at -80°C for further analysis.

Coomassie blue staining: 20 µl of sample from each fraction was applied to SDS-PAGE gels. After electrophoresis at 120 V for 150 minutes, the gel was rinsed with distilled water to remove SDS and buffer salts, and then merged in Coomassie Brilliant Blue G-250 Dye at room temperature. After 10 minutes, the gel was washed by distaining buffer 3 time for 10 minutes each. Fractions containing target protein was collected and condensed to about 500 µl using Amicon® Ultra centrifugal filters (Merk Millipore, Billerica, MA).

Biochemical Assays

Dot blot Hybridization Assay: 2 μl of TGEV or 229E truncated spike proteins (50 μg/ml) were dotted onto a nitrocellulose membrane and dried completely. The blot was blocked in PBST containing 5% non-fat milk at room temperature for 1 hour. The blot were then washed with PBST, and incubated overnight at 4°C with 50 μg/ml pAPN, which had been preincubated alone or with 100uM of APN inhibitors, actinonin (Sigma-Aldrich, St. Louis, MO) or bestatin (Santa Cruz, Dallas, TX). After washed 3 times for 10 minutes, the blot was incubated with anti-His_6 mouse monoclonal IgG_1 antibody (Santa Cruz, Dallas, TX) at 37°C for 2 hours, and then incubated with HRP-conjugated goat anti-mouse IgG antibody (Santa Cruz, Dallas, TX) at 37°C for 1 hour after washed three times with PBST. Finally, the blot was thoroughly washed and detected using ECL Plus (GE Healthcare).

ELISA: Nunc™ MicroWell™ 96-well Microplates (ThermoFisher, Waltham, MA) were coated overnight at 4°C with 100 μg/ml TGEV spike, 5μg/ml MERS-CoV spike or 5 μg/ml SARS-CoV spike. After blocking at room temperature for 2 hours, the plate were incubated at 37°C for 3 hours with 100 μg/ml pAPN, hDPP4 or hACE2. The plate was then treated in the same way as dot-blot hybridization assay with primary and HRP-conjugated secondary antibodies. After washed three times, the plate was incubated with TMB substrate (3, 3', 5, 5'- Tetramethylbenzidine) for 10 minutes, and the reaction was stopped by 1 M H_2SO_4. The color reaction was quantified using Tecan Infinite M1000 PRO Microplate reader at 450 nm.

BLItz: The BLItz (ForteBio, Menlo Park, CA) was used to measure the binding kinetics of CoV spikes with receptors incubated with or without inhibitors at room temperature. Purified spikes in PBS were immobilized on protein A biosensors. Biosensor tips were equilibrated in PBS before associated with receptors preincubated with PBS or inhibitors for 1 hour. Dissociation is then allowed in PBS. The real-time binding process will display in each experiment and analyzed by global fitting.

Table 7. The steps of advanced kinetics experiment in BLItz

Step Type	Duration (seconds)	Position
Initial Baseline	30	Tube (250 µl)
Loading	120	Drop (4 µl)
Baseline	300	Tube (250 µl)
Association	120	Drop (4 µl)
Dissociation	120	Tube (250 µl)

Cell Experiments

Cell lines: The HEK 293T (human embryonic kidney) was obtained from ATCC (www.atcc.org). Huh-7 (human liver) was kindly provided by Charles M. Rice at Rockefeller University and Chien-Te K. Tseng at the University of Texas Medical Branch, respectively. These cell lines were maintained in Dulbecco's modified Eagle medium, supplemented with 10% FBS, 2mM L-glutamine, and 1% penicillin/streptomycin (Life Technologies Inc, Grand Island, NY).

Downstream of endogenous APN in Huh-7 by bestatin with gradient concentration: Huh-7 cells were preincubated with supplemented DMEM media with 0 μM, 10 μM, or 100 μM bestatin (DMSO solution) at 37℃ for 24 hours. The media was then removed and the cells were washed with PBS once. Lysis buffer was added and incubated at room temperature for 30 minutes. The cell lysates were slightly shaken and further analyzed by Western blot.

Downstream of endogenous APN in Huh-7 by inhibitors at different time points: Huh-7 cells were preincubated with supplemented DMEM media with 0 or 100 μM inhibitor (DMSO solution) at 37℃. The cells were harvested as previously described at 0 hour, 1 hour, 2 hours, 4 hours, 8 hours, 12 hours and 24 hours post-treatment and analyzed by Western blot.

Western blot: The level of APN expression in cell lysates was detected by Western blot as previously described.

Reverse- Transcription PCR (RT-PCR): RNA from each sample was extracted by QIAgen® RNeasy Plus Mini Kit. RNA was converted to cDNA using RT-PCR. For each sample, 1 μg of RNA were initially incubated at 70°C for 10 minutes and placed on ice.

20 µl of the reaction mixture was incubated at 37°C for one hour, then heated to 95°C for 5 minutes and stored at 4°C for further use.

Table 8. Reaction mixture of RT-PCR

Component	Volume
Reverse Transcription 10× buffer	2 µl
MgCl2 (25 mM)	4 µl
dNTP mix (2.5 mM each NTP)	8 µl
AMV Reverse Transcriptase (High Conc.)	0.6 µl
Oligo (dT) 15 primer (0.5 µg/ul)	1 µl
RNA (Conc. varies)	1 µg
Nuclease-Free Water to a final volume	20 µl

Real-Time PCR (RT-PCR): APN transcription level was quantified by RT-PCR in StepOnePlus™ Real-Time PCR System (ThermoFisher, Waltham, MA) with SYBR™ Green dye (ThermoFisher, Waltham, MA) from Applied biosystems as sequence detecting reagent. Amplifications were performed in a 10 µl reaction mixture. The reaction an initial denaturation at 95°C, followed by 40 cycles of 15 seconds at 95°C, 15 seconds at 50°C and 1 minute at 72°C. An extension phase of 15 seconds at 95°C and then 1 minute at 60°C was conducted to detect the format of primers annealing. Instant fluorescence was measured in each cycle, and the number of target copies in each reaction was deduced from the threshold cycle (C_T) using Delta Delta C_T method. The number of GAPDH copies was used as a internal control.

Table 9. Primers for RT-PCR

mRNA	upstream	downstream
ANPEP (APN)	CCTGTCATCAATCGGGC	AGTAGCTCAGGCTGCTCAGG
GAPDH	CCATCAATGACCCCTTCATTGACCT	TCTCGCTCCTGGAAGATGGT

Inhibition of APN expression by spikes: HEK 293T cells transiently expressing pAPN were incubated with 20 μg/ml of TGEV spike for 24 hours at 37℃. Huh 7 cells were incubated with 20 μg/ml of HCoV-229E spike for 24 hours at 37℃. The level of APN expression in cell lysates was detected by Western blot as previously described.

Pseudovirus Production: Retroviruses pseudotyped with HCoV-229E spike were generated. A plasmid carrying an env-defective, luciferase-expressing HIV, type 1 genome(pNL4-3.luc.R-E-) and a plasmid encoding HCoV-229E spike were co-transfected into HEK 293T cells using Lipofectamine 3000 reagent (Invitrogen, Carlsbad, CA) according to the instructions of the manufacturer. Supernatants containing pseudoviruses were harvested after 72 hours of transfection. Cell debris were removed by centrifugation.

Pseudovirus Entry: Retrovirus pseudotyped with HCoV-229E Spike or empty vector (mock) were used to transduce Huh 7 cells in 96-well plates. Briefly, cells were preincubated with APN inhibitors in supplemented DMEM (ThermoFisher, Waltham, MA) for 1 hour. After treatment, cells were infected with the pseudovirus in the presence or absence of bestatin (Santa Cruz, Dallas, TX) respectively for 2 hours and subsequently replaced with fresh DMEM (ThermoFisher, Waltham, MA) with or without bestatin (Santa Cruz, Dallas, TX), 10% FBS, L-glutamine, 100 units/ml of penicillin and streptomycin (Invitrogen, Carlsbad, CA). Forty-eight hours later, cells were washed with PBS, lysed, and then transferred to an Optiplate-96 plate (PerkinElmer, Waltham, MA). After Luciferase substrate (Promega, Madison, WI) was added, relative lucifierase units were measured immediately using EnSpire plate reader(PerkinElmer, Waltham, MA).

References

1. **de Groot RJ ea.** 2011. Virus taxonomy: Ninth Report of the International Committee on Taxonomy of Viruses.
2. **Hamre D, Procknow JJ.** 1966. A new virus isolated from the human respiratory tract. Proceedings of the Society for Experimental Biology and Medicine. Society for Experimental Biology and Medicine **121:**190-193.
3. **Fouchier RA, Hartwig NG, Bestebroer TM, Niemeyer B, de Jong JC, Simon JH, Osterhaus AD.** 2004. A previously undescribed coronavirus associated with respiratory disease in humans. Proc Natl Acad Sci U S A **101:**6212-6216.
4. **van der Hoek L, Pyrc K, Jebbink MF, Vermeulen-Oost W, Berkhout RJM, Wolthers KC, Wertheim-van Dillen PME, Kaandorp J, Spaargaren J, Berkhout B.** 2004. Identification of a new human coronavirus. Nature medicine **10:**368-373.
5. **Woo PC, Lau SK, Chu CM, Chan KH, Tsoi HW, Huang Y, Wong BH, Poon RW, Cai JJ, Luk WK, Poon LL, Wong SS, Guan Y, Peiris JS, Yuen KY.** 2005. Characterization and complete genome sequence of a novel coronavirus, coronavirus HKU1, from patients with pneumonia. Journal of virology **79:**884-895.
6. **McIntosh K, Becker WB, Chanock RM.** 1967. Growth in suckling-mouse brain of "IBV-like" viruses from patients with upper respiratory tract disease. Proc Natl Acad Sci U S A **58:**2268-2273.
7. **Ksiazek TG, Erdman D, Goldsmith CS, Zaki SR, Peret T, Emery S, Tong S, Urbani C, Comer JA, Lim W, Rollin PE, Dowell SF, Ling AE, Humphrey CD, Shieh WJ, Guarner J, Paddock CD, Rota P, Fields B, DeRisi J, Yang JY, Cox N, Hughes JM, LeDuc JW, Bellini WJ, Anderson LJ, Group SW.** 2003. A novel coronavirus associated with severe acute respiratory syndrome. The New England journal of medicine **348:**1953-1966.
8. **Rota PA, Oberste MS, Monroe SS, Nix WA, Campagnoli R, Icenogle JP, Penaranda S, Bankamp B, Maher K, Chen MH, Tong S, Tamin A, Lowe L, Frace M, DeRisi JL, Chen Q, Wang D, Erdman DD, Peret TC, Burns C, Ksiazek TG, Rollin PE, Sanchez A, Liffick S, Holloway B, Limor J, McCaustland K, Olsen-Rasmussen M, Fouchier R, Gunther S, Osterhaus AD, Drosten C, Pallansch MA, Anderson LJ, Bellini WJ.** 2003. Characterization of a novel coronavirus associated with severe acute respiratory syndrome. Science **300:**1394-1399.
9. **Zaki AM, van Boheemen S, Bestebroer TM, Osterhaus AD, Fouchier RA.** 2012. Isolation of a novel coronavirus from a man with pneumonia in Saudi Arabia. The New England journal of medicine **367:**1814-1820.
10. **de Groot RJ, Baker SC, Baric RS, Brown CS, Drosten C, Enjuanes L, Fouchier RA, Galiano M, Gorbalenya AE, Memish ZA, Perlman S, Poon LL,**

Snijder EJ, Stephens GM, Woo PC, Zaki AM, Zambon M, Ziebuhr J. 2013. Middle East respiratory syndrome coronavirus (MERS-CoV): announcement of the Coronavirus Study Group. Journal of virology **87:**7790-7792.

11. **Li F.** 2016. Structure, Function, and Evolution of Coronavirus Spike Proteins. Annual review of virology **3:**237-261.
12. **Woo PC, Lau SK, Lam CS, Lau CC, Tsang AK, Lau JH, Bai R, Teng JL, Tsang CC, Wang M, Zheng BJ, Chan KH, Yuen KY.** 2012. Discovery of seven novel Mammalian and avian coronaviruses in the genus deltacoronavirus supports bat coronaviruses as the gene source of alphacoronavirus and betacoronavirus and avian coronaviruses as the gene source of gammacoronavirus and deltacoronavirus. Journal of virology **86:**3995-4008.
13. **Li F.** 2015. Receptor recognition mechanisms of coronaviruses: a decade of structural studies. Journal of virology **89:**1954-1964.
14. **B Schultze CK, M L Ballesteros, L Shaw, R Schauer, L Enjuanes, and G Herrler.** 1996. Transmissible gastroenteritis coronavirus, but not the related porcine respiratory coronavirus, has a sialic acid (N-glycolylneuraminic acid) binding activity. Journal of virology.
15. **Schwegmann-Wessels C, Herrler G.** 2006. Sialic acids as receptor determinants for coronaviruses. Glycoconjugate journal **23:**51-58.
16. **Liu C, Tang J, Ma Y, Liang X, Yang Y, Peng G, Qi Q, Jiang S, Li J, Du L, Li F.** 2015. Receptor usage and cell entry of porcine epidemic diarrhea coronavirus. Journal of virology **89:**6121-6125.
17. **Walls AC, Tortorici MA, Bosch BJ, Frenz B, Rottier PJ, DiMaio F, Rey FA, Veesler D.** 2016. Cryo-electron microscopy structure of a coronavirus spike glycoprotein trimer. Nature **531:**114-117.
18. **Walls AC, Tortorici MA, Frenz B, Snijder J, Li W, Rey FA, DiMaio F, Bosch BJ, Veesler D.** 2016. Glycan shield and epitope masking of a coronavirus spike protein observed by cryo-electron microscopy. Nature structural & molecular biology **23:**899-905.
19. **Yuan Y, Cao D, Zhang Y, Ma J, Qi J, Wang Q, Lu G, Wu Y, Yan J, Shi Y, Zhang X, Gao GF.** 2017. Cryo-EM structures of MERS-CoV and SARS-CoV spike glycoproteins reveal the dynamic receptor binding domains. Nature communications **8:**15092.
20. **Gui M, Song W, Zhou H, Xu J, Chen S, Xiang Y, Wang X.** 2017. Cryo-electron microscopy structures of the SARS-CoV spike glycoprotein reveal a prerequisite conformational state for receptor binding. Cell research **27:**119-129.
21. **Ou X, Guan H, Qin B, Mu Z, Wojdyla JA, Wang M, Dominguez SR, Qian Z, Cui S.** 2017. Crystal structure of the receptor binding domain of the spike glycoprotein of human betacoronavirus HKU1. Nature communications **8:**15216.
22. **Tresnan DB, Holmes KV.** 1998. Feline aminopeptidase N is a receptor for all group I coronaviruses. Coronaviruses And Arteriviruses **440:**69-75.
23. **Oh JS, Song DS, Park BK.** 2003. Identification of a putative cellular receptor 150 kDa polypeptide for porcine epidemic diarrhea virus in porcine enterocytes. Journal of veterinary science **4:**269-275.

24. **Li BX, Ge JW, Li YJ.** 2007. Porcine aminopeptidase N is a functional receptor for the PEDV coronavirus. Virology **365:**166-172.
25. **Kamau AN, Park JE, Park ES, Yu JE, Rho J, Shin HJ.** 2017. Porcine amino peptidase N domain VII has critical role in binding and entry of porcine epidemic diarrhea virus. Virus research **227:**150-157.
26. **Nam E, Lee C.** 2010. Contribution of the porcine aminopeptidase N (CD13) receptor density to porcine epidemic diarrhea virus infection. Veterinary microbiology **144:**41-50.
27. **Shirato K, Maejima M, Islam MT, Miyazaki A, Kawase M, Matsuyama S, Taguchi F.** 2016. Porcine aminopeptidase N is not a cellular receptor of porcine epidemic diarrhea virus, but promotes its infectivity via aminopeptidase activity. The Journal of general virology **97:**2528-2539.
28. **Li W, Luo R, He Q, van Kuppeveld FJM, Rottier PJM, Bosch BJ.** 2017. Aminopeptidase N is not required for porcine epidemic diarrhea virus cell entry. Virus research **235:**6-13.
29. **Delmas B, Gelfi J, Lharidon R, Vogel LK, Sjostrom H, Noren O, Laude H.** 1992. Aminopeptidase-N Is a Major Receptor for the Enteropathogenic Coronavirus Tgev. Nature **357:**417-420.
30. **Tresnan DB, Levis R, Holmes KV.** 1996. Feline aminopeptidase N serves as a receptor for feline, canine, porcine, and human coronaviruses in serogroup I. Journal of virology **70:**8669-8674.
31. **Yeager CL, Ashmun RA, Williams RK, Cardellichio CB, Shapiro LH, Look AT, Holmes KV.** 1992. Human Aminopeptidase-N Is a Receptor for Human Coronavirus-229e. Nature **357:**420-422.
32. **Hofmann H, Pyrc K, van der Hoek L, Geier M, Berkhout B, Pohlmann S.** 2005. Human coronavirus NL63 employs the severe acute respiratory syndrome coronavirus receptor for cellular entry. Proc Natl Acad Sci U S A **102:**7988-7993.
33. **Li WH, Moore MJ, Vasilieva N, Sui JH, Wong SK, Berne MA, Somasundaran M, Sullivan JL, Luzuriaga K, Greenough TC, Choe H, Farzan M.** 2003. Angiotensin-converting enzyme 2 is a functional receptor for the SARS coronavirus. Nature **426:**450-454.
34. **Marzi A, Gramberg T, Simmons G, Moller P, Rennekamp AJ, Krumbiegel M, Geier M, Eisemann J, Turza N, Saunier B, Steinkasserer A, Becker S, Bates P, Hofmann H, Pohlmann S.** 2004. DC-SIGN and DC-SIGNR interact with the glycoprotein of Marburg virus and the S protein of severe acute respiratory syndrome coronavirus. Journal of virology **78:**12090-12095.
35. **Vlasak R, Luytjes W, Spaan W, Palese P.** 1988. Human And Bovine Coronaviruses Recognize Sialic Acid-Containing Receptors Similar To Those Of Influenza C-Viruses. P Natl Acad Sci USA **85:**4526-4529.
36. **Huang X, Dong W, Milewska A, Golda A, Qi Y, Zhu QK, Marasco WA, Baric RS, Sims AC, Pyrc K, Li W, Sui J.** 2015. Human Coronavirus HKU1 Spike Protein Uses O-Acetylated Sialic Acid as an Attachment Receptor Determinant and Employs Hemagglutinin-Esterase Protein as a Receptor-Destroying Enzyme. Journal of virology **89:**7202-7213.

37. **Lu G, Hu Y, Wang Q, Qi J, Gao F, Li Y, Zhang Y, Zhang W, Yuan Y, Bao J, Zhang B, Shi Y, Yan J, Gao GF.** 2013. Molecular basis of binding between novel human coronavirus MERS-CoV and its receptor CD26. Nature **500:**227-231.
38. **Williams RK, Jiang GS, Holmes KV.** 1991. Receptor for Mouse Hepatitis-Virus Is a Member Of the Carcinoembryonic Antigen Family Of Glycoproteins. P Natl Acad Sci USA **88:**5533-5536.
39. **Williams RK, Jiang GS, Snyder SW, Frana MF, Holmes KV.** 1990. Purification of the 110-kilodalton glycoprotein receptor for mouse hepatitis virus (MHV)-A59 from mouse liver and identification of a nonfunctional, homologous protein in MHV-resistant SJL/J mice. Journal of virology **64:**3817-3823.
40. **Schultze B, Cavanagh D, Herrler G.** 1992. Neuraminidase Treatment Of Avian Infectious-Bronchitis Coronavirus Reveals a Hemagglutinating Activity That Is Dependent on Sialic Acid-Containing Receptors on Erythrocytes. Virology **189:**792-794.
41. **Belsham GJ, Rasmussen TB, Normann P, Vaclavek P, Strandbygaard B, Botner A.** 2016. Characterization of a Novel Chimeric Swine Enteric Coronavirus from Diseased Pigs in Central Eastern Europe in 2016. Transboundary and emerging diseases **63:**595-601.
42. **Kim L, Hayes J, Lewis P, Parwani AV, Chang KO, Saif LJ.** 2000. Molecular characterization and pathogenesis of transmissible gastroenteritis coronavirus (TGEV) and porcine respiratory coronavirus (PRCV) field isolates co-circulating in a swine herd. Archives of virology **145:**1133-1147.
43. **Bradburne AF, Bynoe ML, Tyrrell DA.** 1967. Effects of a "new" human respiratory virus in volunteers. British medical journal **3:**767-769.
44. **Pene F, Merlat A, Vabret A, Rozenberg F, Buzyn A, Dreyfus F, Cariou A, Freymuth F, Lebon P.** 2003. Coronavirus 229E-related pneumonia in immunocompromised patients. Clinical infectious diseases : an official publication of the Infectious Diseases Society of America **37:**929-932.
45. **Dijkman R, van der Hoek L.** 2009. Human Coronaviruses 229E and NL63: Close Yet Still So Far. J Formos Med Assoc **108:**270-279.
46. **Mina-Osorio P.** 2008. The moonlighting enzyme CD13: old and new functions to target. Trends in molecular medicine **14:**361-371.
47. **Su L, Cao J, Jia Y, Zhang X, Fang H, Xu W.** 2012. Development of Synthetic Aminopeptidase N/CD13 Inhibitors to Overcome Cancer Metastasis and Angiogenesis. ACS medicinal chemistry letters **3:**959-964.
48. **Hashida H, Takabayashi A, Kanai M, Adachi M, Kondo K, Kohno N, Yamaoka Y, Miyake M.** 2002. Aminopeptidase N is involved in cell motility and angiogenesis: Its clinical significance in human colon cancer. Gastroenterology **122:**376-386.
49. **Chen L, Lin YL, Peng G, Li F.** 2012. Structural basis for multifunctional roles of mammalian aminopeptidase N. Proc Natl Acad Sci U S A **109:**17966-17971.

50. **Wong AH, Zhou D, Rini JM.** 2012. The X-ray crystal structure of human aminopeptidase N reveals a novel dimer and the basis for peptide processing. The Journal of biological chemistry **287:**36804-36813.
51. **Delmas B, Gelfi J, Kut E, Sjostrom H, Noren O, Laude H.** 1994. Determinants Essential for the Transmissible Gastroenteritis Virus-Receptor Interaction Reside within a Domain Of Aminopeptidase-N That Is Distinct From the Enzymatic Site. Journal of virology **68:**5216-5224.
52. **Santiago C, Mudgal G, Reguera J, Recacha R, Albrecht S, Enjuanes L, Casasnovas JM.** 2017. Allosteric inhibition of aminopeptidase N functions related to tumor growth and virus infection. Scientific reports **7:**46045.
53. **Umezawa H, Aoyagi T, Suda H, Hamada M, Takeuchi T.** 1976. Bestatin, an inhibitor of aminopeptidase B, produced by actinomycetes. The Journal of antibiotics **29:**97-99.
54. **Bauvois B, Dauzonne D.** 2006. Aminopeptidase-N/CD13 (EC 3.4.11.2) inhibitors: chemistry, biological evaluations, and therapeutic prospects. Medicinal research reviews **26:**88-130.
55. **Rich DH, Moon BJ, Harbeson S.** 1984. Inhibition of aminopeptidases by amastatin and bestatin derivatives. Effect of inhibitor structure on slow-binding processes. Journal of medicinal chemistry **27:**417-422.
56. **Zhang X, Fang H, Zhang J, Yuan Y, Xu W.** 2011. Recent advance in aminopeptidase N (APN/CD13) inhibitor research. Current medicinal chemistry **18:**5011-5021.
57. **Tieku S, Hooper NM.** 1992. Inhibition of aminopeptidases N, A and W. A re-evaluation of the actions of bestatin and inhibitors of angiotensin converting enzyme. Biochemical pharmacology **44:**1725-1730.
58. **Raj VS, Mou H, Smits SL, Dekkers DH, Muller MA, Dijkman R, Muth D, Demmers JA, Zaki A, Fouchier RA, Thiel V, Drosten C, Rottier PJ, Osterhaus AD, Bosch BJ, Haagmans BL.** 2013. Dipeptidyl peptidase 4 is a functional receptor for the emerging human coronavirus-EMC. Nature **495:**251-254.
59. **Wang N, Shi X, Jiang L, Zhang S, Wang D, Tong P, Guo D, Fu L, Cui Y, Liu X, Arledge KC, Chen YH, Zhang L, Wang X.** 2013. Structure of MERS-CoV spike receptor-binding domain complexed with human receptor DPP4. Cell research **23:**986-993.
60. **Dales NA, Gould AE, Brown JA, Calderwood EF, Guan B, Minor CA, Gavin JM, Hales P, Kaushik VK, Stewart M, Tummino PJ, Vickers CS, Ocain TD, Patane MA.** 2002. Substrate-based design of the first class of angiotensin-converting enzyme-related carboxypeptidase (ACE2) inhibitors. Journal of the American Chemical Society **124:**11852-11853.
61. **Kuba K, Imai Y, Rao S, Gao H, Guo F, Guan B, Huan Y, Yang P, Zhang Y, Deng W, Bao L, Zhang B, Liu G, Wang Z, Chappell M, Liu Y, Zheng D, Leibbrandt A, Wada T, Slutsky AS, Liu D, Qin C, Jiang C, Penninger JM.** 2005. A crucial role of angiotensin converting enzyme 2 (ACE2) in SARS coronavirus-induced lung injury. Nature medicine **11:**875-879.

62. **Reguera J, Santiago C, Mudgal G, Ordono D, Enjuanes L, Casasnovas JM.** 2012. Structural bases of coronavirus attachment to host aminopeptidase N and its inhibition by neutralizing antibodies. PLoS pathogens **8:**e1002859.
63. **Wilkes SH, Prescott JM.** 1985. The slow, tight binding of bestatin and amastatin to aminopeptidases. The Journal of biological chemistry **260:**13154-13162.
64. **Wu K, Chen L, Peng G, Zhou W, Pennell CA, Mansky LM, Geraghty RJ, Li F.** 2011. A virus-binding hot spot on human angiotensin-converting enzyme 2 is critical for binding of two different coronaviruses. Journal of virology **85:**5331-5337.
65. **Towler P, Staker B, Prasad SG, Menon S, Tang J, Parsons T, Ryan D, Fisher M, Williams D, Dales NA, Patane MA, Pantoliano MW.** 2004. ACE2 X-ray structures reveal a large hinge-bending motion important for inhibitor binding and catalysis. The Journal of biological chemistry **279:**17996-18007.
66. **Pelchen-Matthews A, Signoret N, Klasse PJ, Fraile-Ramos A, Marsh M.** 1999. Chemokine receptor trafficking and viral replication. Immunological reviews **168:**33-49.